Grid Generation and Inviscid Flow Computation About a Cranked-Winged Airplane Geometry

L.-E. Eriksson*
Old Dominion University, Norfolk, Virginia
R. E. Smith†
NASA Langley Research Center, Hampton, Virginia
and
M. R. Wiese‡ and N. Farr§
Computer Sciences Corporation, Hampton, Virginia

An algebraic grid generation procedure that defines a patched multiple-block grid system suitable for a fighter-type airplane geometry is described. The grid generation is based entirely on transfinite interpolation and is computationally efficient. Grids are presented for an experimental aircraft with a fuselage, including an engine inlet, 70–20 deg cranked delta wing, canard, and a vertical tail fin. A finite-volume Euler solver using explicit Runge-Kutta time-stepping is adapted to the grid system and implemented on a supercomputer with a high degree of vectorization. Computed inviscid compressible flow solutions about the fighter configuration are presented for Mach 2 at 3.79, 7, and 10 deg angles of attack. Comparisons between the present numerical solutions, other numerical experiments, and wind-tunnel measurements indicate that the described approach is viable to simulate inviscid compressible flow about complex airplane geometries.

Introduction

IT has become possible to solve inviscid compressible flow routinely using the Euler equations for moderately complex geometries.[1–4] However, most of the three-dimensional computations that have been made use single-block structured grids.[5] For very complex geometries, either an unstructured grid or multiple-block structured grids that are patched together or overlapped are required. Several papers[6–12] have been published recently on this subject, and it is clear that there are different strategies that can be pursued.

The grid generation strategy followed herein is to patch together several boundary-fitted grids with C^1 continuity, and, henceforth, all grids that are described are structured. This approach keeps the flow solution procedure almost as simple as on a single-block grid, since block interface points can be treated as interior points in neighboring blocks. The grid topology that is used attempts to minimize the number of grid blocks and the amount of grid skewness. The grid generation procedure is algebraic and is based entirely on transfinite interpolation,[13] and since the grid computation is direct, the procedure is computationally efficient. The computation of the surface grid of a configuration is considered as a separate problem, and once the grid topology is decided upon, the surface grid is computed using the techniques described in Ref. 14. A time-marching finite-volume scheme[1–4,15] has been adapted to the multiple-grid system and has been highly vectorized.

In Ref. 16, the basic grid generation concept and calculations on simplified prototype models are presented. In the following sections, the grid generation and Euler solution procedure are described for an accurate representation of an advanced fighter airplane geometry with a fuselage, including an engine inlet, canard, 70–20 deg cranked delta wing and vertical tail fin (Fig. 1). Using the Euler procedure, solutions are obtained for Mach 2 at 3.79, 7, and 10 deg angles of attack. The characteristics of the solutions are discussed, and contour plots of the pressure coefficient on the configuration surface are presented for the three cases. The pressure coefficient at specific cross sections for the 3.79 deg case is compared with an available full potential solution[17] and an Euler solution.[18] Force calculations are obtained from the numerical solutions and compared with experimental observations described in Ref. 19. The initial Euler solution for the 10 deg angle of attack case exhibited an oscillation near the leading edge of the 70 deg swept part of the wing. The convergence procedure for the finite-volume approach was modified and a steady-state solution obtained. Possible reasons for the occurrence of the oscillation are discussed.

Grid Generation

Grid Topology

For an advanced fighter-type airplane configuration such as the one shown in Fig. 1, only patched C^1-continuous grids are considered, and grid lines are required to conform to all wing edges. There are two basic alternative topologies (Fig. 2) that can be enforced. The simplest approach is to let selected outgoing grid lines conform to the leading and trailing edges of both the canard and the wing. For a cranked delta wing with a highly swept inner region, it is clear that this type of grid has disadvantages. Not only is the grid highly skewed at the leading edge of the inner part of the wing, but its structure makes it difficult to concentrate grid points in a smooth fashion in the apex region of the wing. A different approach is to let the leading edge of the inner wing be represented by a grid line associated with two grid systems as shown in Fig. 2. It is clear that this "dual-block" topology gives a less skewed grid and also gives a natural concentration of grid points in the apex region of the wing. In the resulting dual-block grid, the third family of grid lines wraps around the fuselage, and both lifting surfaces can be represented as interior slits, with the inner wing slit in the inner grid and the canard and outer wing slits in the outer grid.

Presented as Paper 87-1125 at the AIAA 8th Computational Fluid Dynamics Conference, Honolulu, HI, June 9–11, 1987; received Aug. 31, 1987; revision received Oct. 2, 1987. Copyright © American Institute of Aeronautics and Astronautics, Inc., 1987. All rights reserved.

*Research Associate Professor.
†Senior Research Engineer. Member AIAA.
‡Senior Member, Technical Staff.
§Member, Technical Staff.

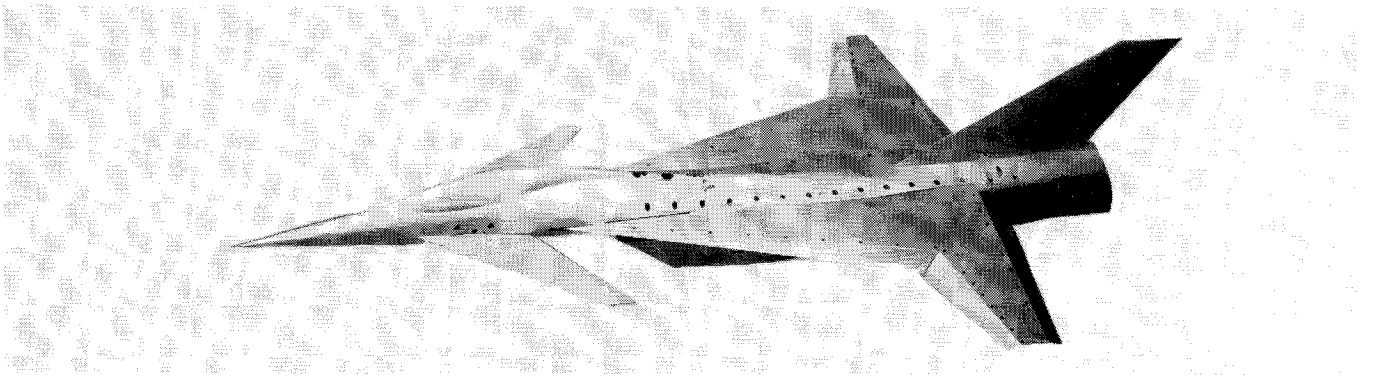

Fig. 1 An advanced fighter aircraft configuration.

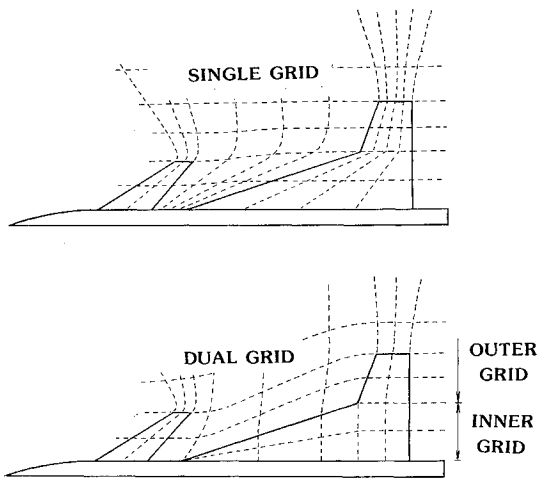

Fig. 2 Alternate grid topologies.

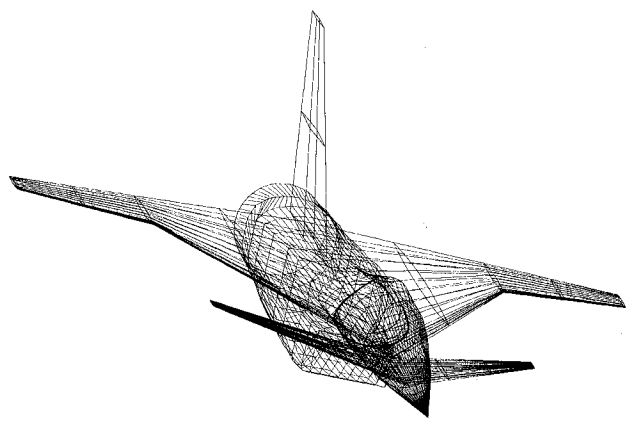

Fig. 3 Component description of the fighter configuration.

Surface Grid

After deciding on the grid topology, the nex step is the computation of a suitable surface grid that defines the airplane geometry and conforms to the chosen grid topology. The surface grid computation is performed using a set of computer programs that have been developed specifically for aircraft surface geometry. In general, a configuration is defined by cross sections for each component (i.e., fuselage, wing, canard, tail; see Fig. 3). A bicubic representation of each component is established by fitting cubic splines along and across the defining cross sections.[14] The intersection of components such as the wing and fuselage is obtained by simultaneously solving for the intersection of the bicubic patch representation of the intersecting components and a sequence of planes. Similarly, grid curves on the surface of a component are computed using the patch-plane intersection approach. Finally, grid points are distributed along the intersection curves using single-valued functions relating grid points to arc length. Figure 4 shows the fighter surface grid for the bottom dual-block and the top dual-block. In the windward direction the grid is concentrated near the leading and trailing edges of the canard and across the fuselage and wing, corresponding to the leading and trailing edges of the 20 deg swept portion of the wing. The grid is concentrated at the leading edge of the 70 deg swept portion of the wing and across the rear of the wing at the dual-block intersection. Around the surface, the grid is concentrated at the intersection of the top and bottom blocks.

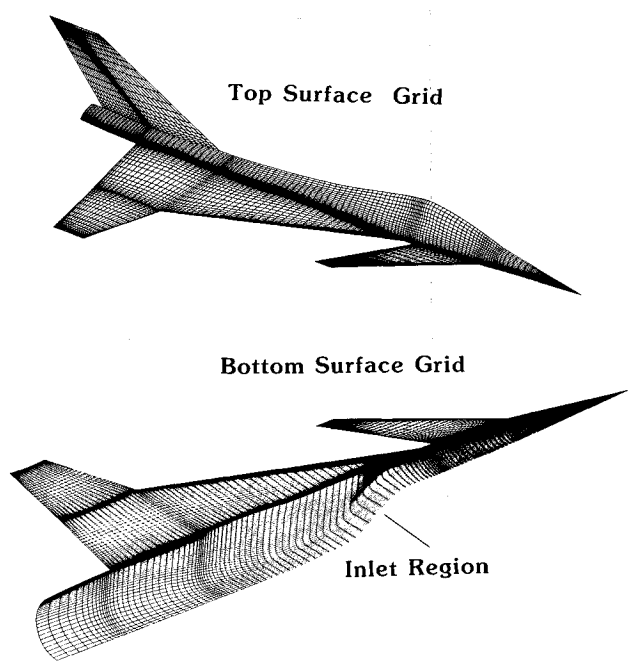

Fig. 4 Grid description of the aircraft surface.

Exterior Grid Generation

Once a satisfactory surface grid is defined, the next task is to extend the surface grid out into the flowfield. The complete grid is computed by first dividing it into several subgrids and then "filling in" one subgrid after the other by transfinite interpolation.[13] Transfinite interpolation is a technique where the desired multivariate interpolation operator is defined as the Boolean sum of several univariate interpolations. For each subgrid, some of the six bounding surfaces are obtained from

the surface grid or from previously computed adjoining subgrids, and some are constructed by simple analytic functions. C^1-continuity between subgrids is achieved by using derivative information as well as positional information in the interpolation. Grid point concentration is achieved by the appropriate definition of the blending functions.[13]

The subgrids closest to the fuselage are computed first and the outermost subgrids last. For the fuselage/wing/canard/tail configuration there are 20 interpolation steps and subgrids. The subgrids are only partitions of the actual grid arrays and are merged into a dual-block about the bottom of the configuration and a dual-block about the top.

Fighter Configuration

The fuselage of the configuration of interest (Fig. 1) has an integrated canopy over the cockpit, an engine inlet separated from the main part of the fuselage by a boundary layer diverter, and the midsection is area ruled for supersonic flow. The canards and wings are defined by parabolic arc streamwise sections, and the cranked wing is swept 70 deg followed by 20 deg. The intersection of the wing leading edge and the fuselage is near the vertical center of the fuselage, and the intersection of the wing trailing edge and the fuselage is near the top of the fuselage. The vertical fin intersects the fuselage in much the same way as the canard except that it is defined vertically rather than spanwise. The grid about the fighter configuration is divided into a bottom grid and a top grid, and the common grid surface is H-type with identical grid points except on the wing and canard.

Both the bottom and top grids are dual-block grids as described above. The inner blocks covers the region around the inner part of the wing and the aft part of the fuselage and vertical tail (Fig. 5). The outer grid covers the region around the forward part of the fuselage, canard and the outer part of the wing (Fig. 6). Figure 7 shows that C^1-continuity between the inner and outer grids cannot be enforced all the way to the singularity at the wing apex caused by the particular topology. However, this "irregular" region around the singular ring can be made arbitrarily small to keep the truncation error at a tolerable level.

An accurate modeling of the fuselage inlet and boundary layer diverter region is not attempted at this time and will require additional grid blocks. Instead, the geometry is simplified by filling in the boundary layer diverter region between the fuselage and inlet and by forcing certain grid lines to run along the slightly rounded inlet edge. The major influence of the inlet is accounted for by flow through boundary conditions at those grid cells that coincide with the inlet opening. In Fig. 4, the region of the grid cells corresponding to the engine inlet are pointed out. Figure 8 shows the extension of the grid from the configuration boundary to the outer boundary.

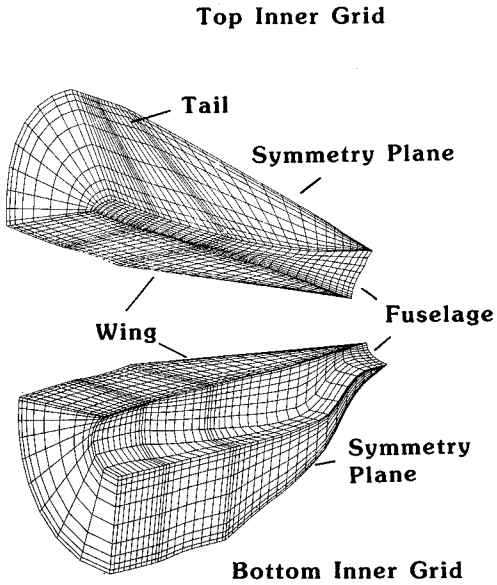

Fig. 5 Inner grid-blocks for a dual-block topology.

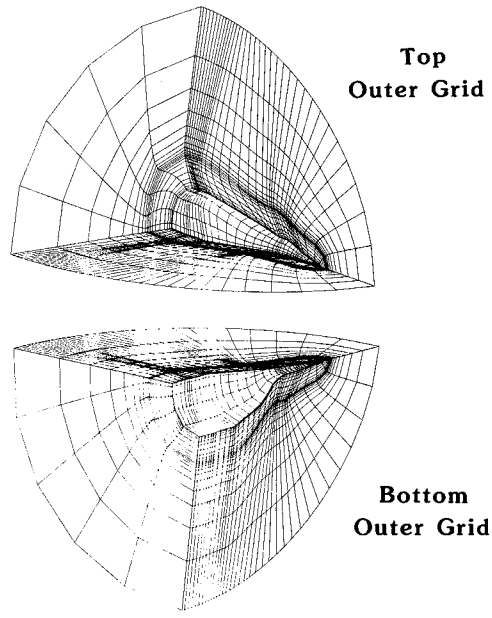

Fig. 6 Outer grid blocks for a dual-block topology.

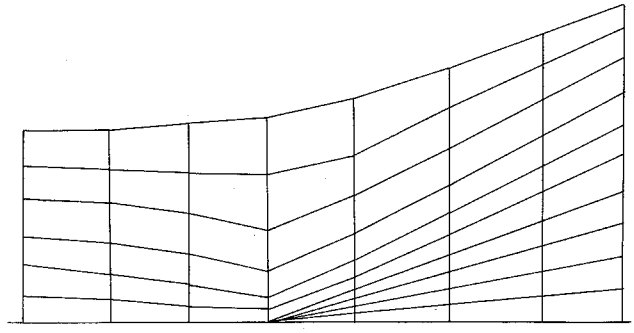

Fig. 7 Detail of the intersection between grids.

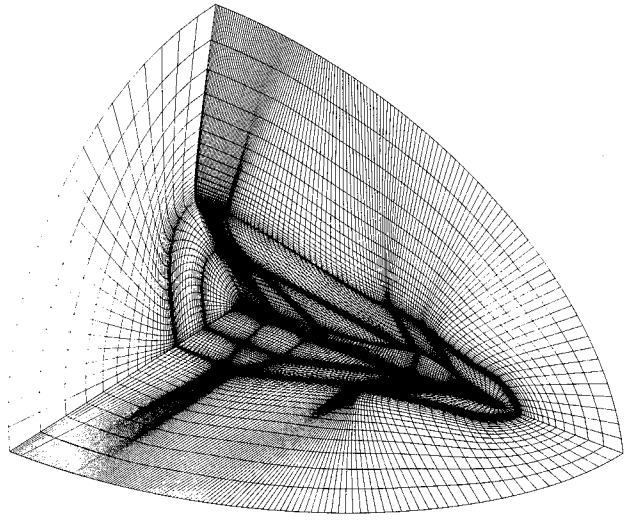

Fig. 8 Grid surfaces extending from the configuration boundary to the outer boundary.

Euler Flow Solution

Numerical Method

The numerical solution of the Euler equations is based on a centered finite-volume scheme with explicit Runge-Kutta time stepping.[1-4,16] This type of scheme was first used by Jameson et al.,[16] but the present scheme differs significantly from this original scheme, mainly in the definition of the damping terms and the farfield boundary conditions.

The finite-volume scheme is derived by applying the full Euler equations in integral form to each hexahedral grid cell and making consistent approximations of both the volume and surface integrals. For the center-of-cell formulation, the resulting semidiscrete scheme is written:

$$\mathrm{VOL}_{i,j,k}(\mathrm{d}/\mathrm{d}t)q_{i,j,k} + F_{i+1/2,j,k} - F_{i-1/2,j,k} + G_{i,j+1/2,k} - G_{i,j-1/2,k} + H_{i,j,k+1/2} - H_{i,j,k-1/2} = 0 \quad (1)$$

In Eq. (1), $q_{i,j,k}$ denotes the flow-state vector containing density, momentum (x,y,z components), and energy at the center of cell (i,j,k). $\mathrm{VOL}_{i,j,k}$ denotes the volume of grid cell (i,j,k) and $F_{i+1/2,j,k}$, $G_{i,j+1/2,k}$, $H_{i,j,k+1/2}$ denote the approximate integrated flux of mass, momentum, and energy through the six cell walls of grid cell (i,j,k). These integrated fluxes are computed by taking the average of the nonlinear flux functions evaluated at cell centers and multiplying these quantities with the normal vector and surface area of the appropriate wall cell. Since the flux computations are symmetric, the resulting scheme is completely centered. The semidiscrete scheme [Eq. (1)] is conservative and second-order accurate on a smooth grid, but it is also completely nondissipative due to the symmetric flux computations. In order to suppress aliasing and shock-induced oscillations, a mixture of second-difference and fourth-difference damping terms is added to Eq. (1). Here, the fourth-difference terms are global and linear, whereas, the pressure-controlled second-difference terms are nonlinear and are only activated around shocks.

An explicit three-stage Runge-Kutta scheme is used to integrate Eq. (1) in time. Since only steady-state solutions are desired, the concept of local time stepping is used to accelerate the convergence to steady state.

Boundary Conditions

There are three types of boundary conditions at solid walls, only pressure is needed and is obtained by linear extrapolation from the two nearest cell centers. At grid interfaces of C^1-continuous type, the interior scheme is still used, but necessary flow information for cell centers outside the current grid domain is obtained from the neighboring grid domain. At inflow/outflow boundaries, an absorbing condition based on the theory of Engquist and Majda[20] is applied.

Computer Implementation

Surface and Exterior Grids

The surface grid is computed independently after the topology, the number of grid points in the two coordinate directions on the surface, and the concentrations of grid points has been decided upon. The surface grid is stored in a file to be used as input for the exterior grid.

The exterior grid generation is performed in a program that uses the surface grid and control parameters as input. The program is written in FORTRAN-77 and will run on any number of computers depending on the size of the grid. For the grid around the experimental fighter configuration used for the solutions described later, there are 309,120 grid points. The unvectorized exterior grid generation program is run on a vector supercomputer to compute the grid point coordinates and corresponding cell volumes. This program is run on the supercomputer because of the large amount of storage required for the grid, and the output of the program is the input for the Euler code.

Euler Solver

The finite-volume scheme has been implemented on a vector supercomputer for the dual-block grid topology. By vectorizing in planes, a computational speed ten times that of the scalar version is achieved for vector lengths around 1000. The CPU time for one complete time step is 9.5 s for 309,120 grid points. This corresponds to a processing time of 3.07×10^{-5} s per grid point per time step.

Computational Results

The grid generation scheme and Euler solver described above have been applied to a generic fuselage/wing/canard configuration[15] and the experimental fighter configuration. A description of three flowfield solutions over the fighter configuration at Mach 2 and angles of attack of 3.79, 7, and 10 deg are presented. A steady solution is assumed to be achieved when the maximum residual (change in density) from one step to the next is less than 1×10^{-5}.

Mach 2—Angle of Attack 3.79 Deg

For a freestream Mach number of 2.0 and 3.79 deg angle of attack, a steady-state solution is achieved after 800 steps, using freestream initial conditions. Pressure coefficient contours on the top and bottom surfaces of the fuselage, canard, and wing are shown in Fig. 9. Figure 10 shows shaded contours of the pressure coefficient on three surfaces in the streamwise direction. The figures show all the expected features of the flow, such as high pressure in front of the canopy and low pressure behind it, low pressure along the upper leading edge of the inner wing, and high pressure under the outer wing. An important feature is the continuation of the low-pressure region along the top leading edge of the inner wing to the region between the outer and inner wing, downstream of the crank. This indicates that there is some vortex generation (thus, entropy increases at the inner-wing leading edge).

The flow enters the inlet region in a smooth manner, but there is considerable increase in pressure. There is also a high-pressure region on the fuselage and bottom wing surface just downstream of the inlet. There is a bulging (area ruling) of the fuselage behind the inlet that gives rise to this high pressure.

Mach 2—Angle of Attack 7 Deg

Increasing the angle of attack to 7 deg while holding the Mach number at 2 causes the pressure to increase on the bottom of the configuration and decrease on the top (Fig. 11). On the top wing

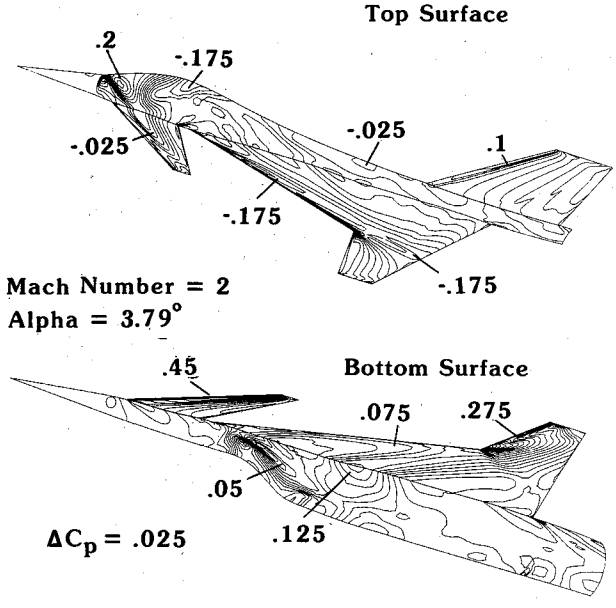

Fig. 9 Contours of pressure coefficient C_p on the aircraft surface.

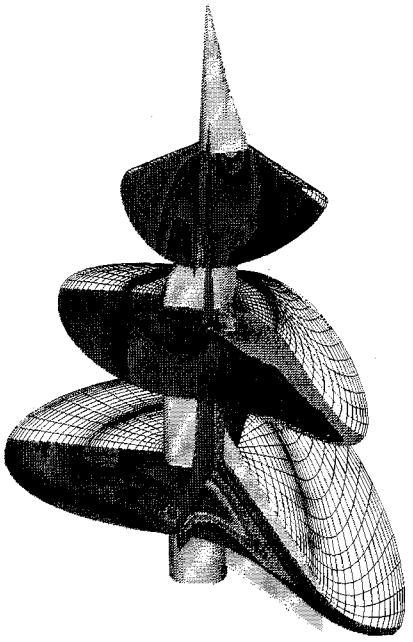

Fig. 10 Shaded levels of the pressure coefficient on three windward surfaces, Mach = 2, angle of attack = 3.79 deg.

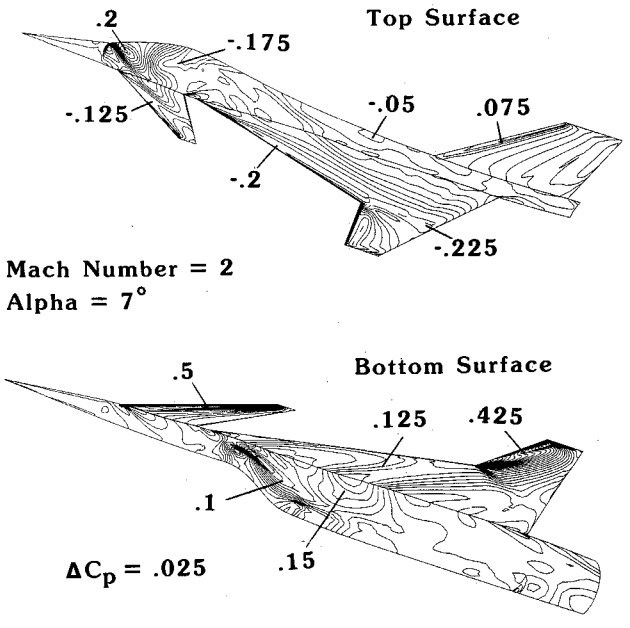

Fig. 11 Contours of pressure coefficient, angle of attack = 7 deg.

surface there is strong indication of vortical flow in the pressure distribution. Another interesting point to note is that on the bottom surface, the high-pressure region emanating from the bulge on the fuselage has moved forward on the bottom of the wing. The initial conditions for this case are the results of the 3.79 deg case, and convergence occurs in 500 steps.

Mach 2—Angle of Attack 10 Deg

Increasing the angle of attack from 3.79 to 10 deg while holding the Mach number at 2 is the second case in chronological order that was attempted for the fighter configuration. The initial conditions are those of the 3.79 deg angle-of-attack solution. At first, convergence toward a steady-state solution appeared normal with residuals decreasing at the expected rate. However, before converging the root-mean-square residual

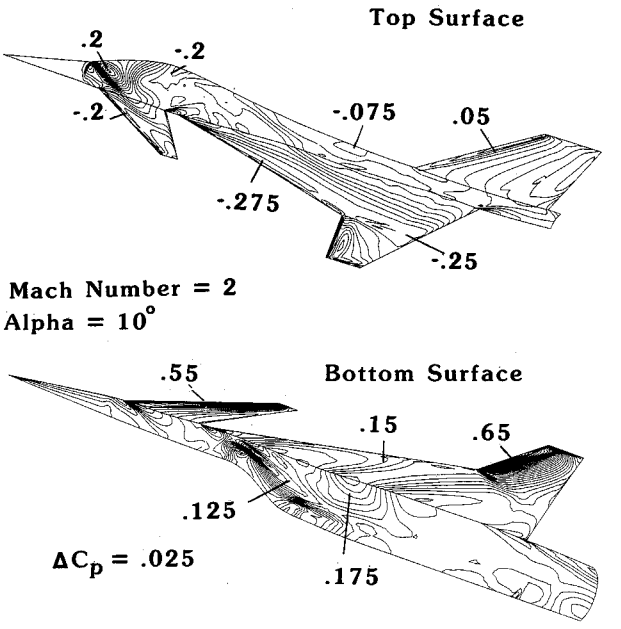

Fig. 12 Contours of pressure coefficient, angle of attack = 10 deg.

and the maximum residual leveled off and began oscillating. Investigation of the pressure coefficient indicates that the high residuals emanate from the top grid just inside the leading edge of the 70 deg swept portion of the wing. Elsewhere, the residuals are well below the cutoff limit. Since the residuals appeared to be near periodic with period approximately 100 steps, a sequence of images (pressure solution on the top of the wing) was created for 400 steps and stored on video tape. Playing back the video shows an oscillation in the pressure just inside the leading edge of the highly-swept portion of the wing emanating midway between the apex of the wing and the crank and propagating both upstream and downstream. There is no physical explanation for this deviation from a steady-state solution, although the shock from the bulge on the bottom surface impinges near this point. The oscillation does not occur on the generic model at Mach 2 and 10 deg angle of attack where there is no irregularity in the fuselage (a steady state is reached[15]).

The Euler solver applied in this study uses local time stepping, and it is hypothesized that the unsteady solution is the result of this numerical approach coupled with the given grid and physics. To test this contention, the Euler solver was modified to run at the minimal time step everywhere. The solution converged to less than the allowable residual at all the grid cells, but very slowly. This indicates that the oscillation problem can be overcome with global time stepping but does not proclaim to be the only solution. The 7 deg angle-of-attack case was computed using local time stepping after having difficulty with the 10 deg case. No unsteady phenomena were observed.

Figure 12 shows the steady state pressure coefficient solution at Mach 2 and 10 deg angle of attack. The pressure increases on the bottom surface and decreases on the top surface. Strong vortical motion is evident on the top wing surface, and the high-pressure region, emanating from the bulge on the fuselage, moves forward on the wing.

Comparison with Other Data

Comparisons of the present computation with corresponding results of a full potential method[17] and another Euler solution[18] with a completely different grid are made. Figures 13 and 14 show the spanwise pressure distribution at constant-x sections at the canard and the highly swept portion of the wing. In general, the agreement is good at these stations.

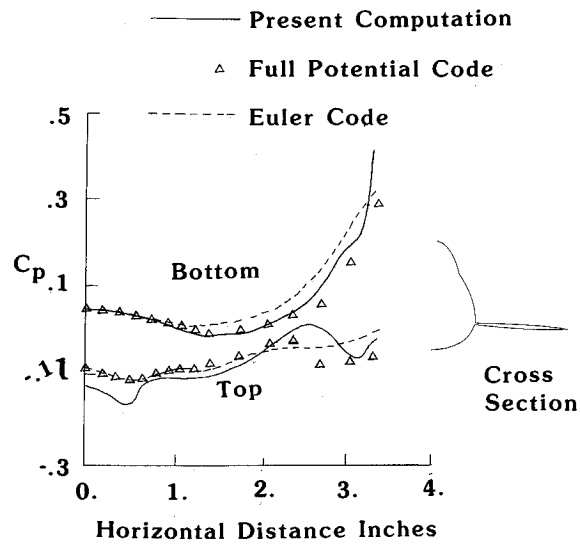

Fig. 13 Pressure coefficient across the canard.

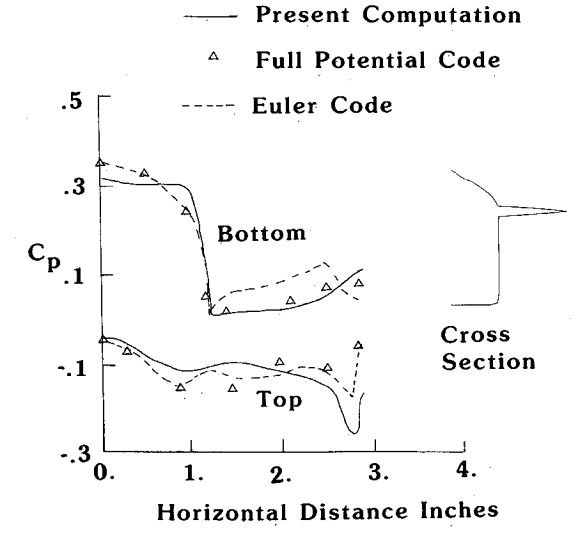

Fig. 14 Pressure coefficient across the fuselage and wing at the engine inlet.

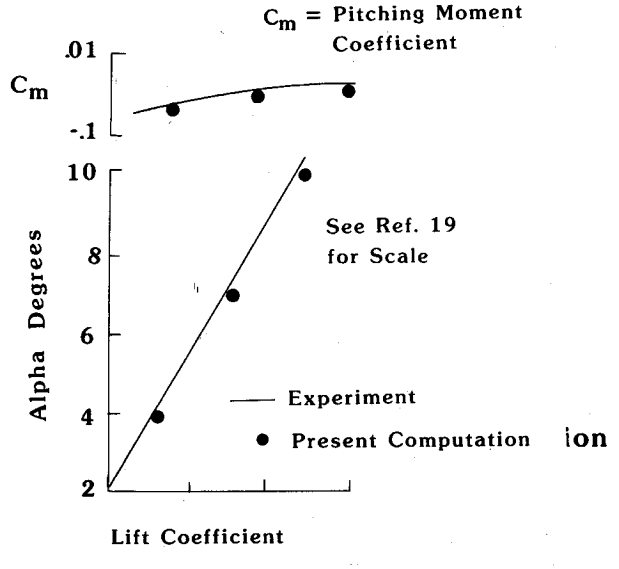

Fig. 15 Lift and pitching moment.

Reference 19 describes a series of wind-tunnel experiments between Mach 1.6 and 2.5 using the configuration shown in Fig. 1 and other geometric variations. In the experiments, the model was instrumented only to measure body forces. The pressure solutions on the surface grid obtained in this numerical study at Mach 2 and 3.79, 7, and 10 deg angles of attack were integrated accounting for flow into the engine inlet. The lift coefficient and pitching moment coefficient were computed and are shown in comparison with those obtained in the physical experiments in Fig. 15. The agreement of these two force characteristics from the physical and numerical experiments is quite good. There does appear, however, to be a bias over the range of the angle of attack, and this is attributed to removal of the boundary-layer diverter in modeling the surface grid in the engine inlet region.

Conclusions

The computational results obtained demonstrate that the grid system used here and the finite-volume Euler solver is a viable approach to the problem of simulating the compressible flow around a complex fighter-type airplane geometry at moderate angles of attack. Due to the natural concentration of grid points in the wing apex region given by this grid topology, it is possible to capture the vortex generated at the sharp leading edge. The results of the present computations at Mach 2 and 3.79 deg angle of attack are in good agreement with those of a full potential method and another Euler solution. The force calculations made in the present numerical experiments compare favorably with those measured in wind-tunnel experiments. At Mach 2 and 10 deg angle of attack a converged solution is obtained with global time stepping to avoid an oscillation that occurred with local time stepping.

References

[1]Rizzi, A. W. and Eriksson, L.-E., "Computation of Flow Around Wings Based on the Euler Equations," *Journal of Fluid Mechanics*, Vol. 148, Nov. 1984, pp. 45–71.

[2]Eriksson, L.-E. and Rizzi, A. W., "Computation of Vortex Flow Around a Canard/Delta Combination," *Journal of Aircraft*, Vol. 21, Nov. 1984, pp. 858–865.

[3]Rizzi, A. and Eriksson, L.-E., "Computation of Inviscid Incompressible Flow with Rotation," *Journal of Fluid Mechanics*, Vol. 153, April, 1985, pp. 275–312.

[4]Eriksson, L.-E., "Simulation of Inviscid Flow Around Airfoils and Cascades Based on the Euler Equations," FFA TN-1985-20, Stockholm, Sweden, June, 1985.

[5]Smith, R. E. and Eriksson, L.-E., "Algerbraic Grid Generation," *Computer Methods in Applied Mechanics and Engineering*, Aeronautical Research Inst. of Sweden, North Holland, Vol. 64, 1987, pp. 285–300.

[6]Rai, M. M., "A Conservative Treatment of Zonal Boundaries for Euler Equation Calculations," AIAA Paper 84-0164, Jan. 1984.

[7]Karman, S. L. Jr., Steinbrenner, J. P., and Kisielewski, K. M., "Analysis of the F-16 Flow Field by a Block Grid Euler Approach," 58th Meeting of the Fluid Dynamics Panel Symposium on Applications of Computational Fluid Dynamics in Aeronautics, Aix-En-Provence, France, April, 1986.

[8]Weatherill, N. C. and Forsey, C. R., "Grid Generation and Flow Calculations for Complex Aircraft Geometrics Using a Multi-Block Scheme," AIAA Paper 84-1665, July, 1984.

[9]Berger, M. J. and Jameson, A., "Automatic Adaptive Grid Refinement for the Euler Equations," Department of Mechanical and Aerospace Engineering, MAE Rept. 1633, Princeton University, Princeton, NJ, Oct. 1983.

[10]Eriksson, L.-E., "Euler Solutions on 0-0 Grids Around Wings Using Local Refinement," *Proceedings of the 6th GAMM Conference on Numerical Methods in Fluid Mechanics*, D. Rues & W. Kordulla, eds., Vieweg Verlag, Gottingen, Germany.

[11]Benek, J. A., Buning, P. G., and Steger, J. L., "A 3-D Chimera Grid Embedding Technique," AIAA Paper 85-1523, July, 1985.

[12]Fritz, W. and Leicher, S., "Numerical Solution of 3-D Inviscid Flow Fields Around Complete Aircraft Configurations," 15th Congress International Council of the Aeronautical Sciences, London, UK, Sept. 1986.

[13]Eriksson, L.-E., "Practical Three-Dimensional Mesh Generation Using Transfinite Interpolation," *SIAM Journal on Scientific and Statistical Computing*, Vol. 6, No. 3, July 1985, pp. 712–741.

[14]Smith, R. E., Kudlinski, R. A., Everton, E. L., and Wiese, M. R., "Algebraic Grid Generation About Wing-Fuselage Bodies," *Journal of Aircraft*, Vol. 24, Dec. 1987, pp. 868–872.

[15]Eriksson, L.-E., "Flow Solution on a Dual-Block Grid Around an Airplane," *Computer Methods in Applied Mechanics and Engineering*, North-Holland, Vol. 64, Oct. 1987, pp. 79–93.

[16]Jameson, A., Schmidt, W., and Turkel, E., "Numerical Solutions of the Euler Equations by Finite Volume Methods Using Runge-Kutta Time-Stepping Schemes," AIAA Paper 81-1259, June 1981.

[17]Szema, K.-Y. and Shankar, V., "Validation of a Full Potential Method for Combined Yaw and Angle of Attack," AIAA Paper 86–1834, June 1986.

[18]Szema, K.-Y. and Chakravarthy, S. R., "Multi-Zone Euler Marching Technique for Flow Over Single and Multi-Body Configurations," AIAA Paper 87-0592, Jan. 1987.

[19]Hom, K. W. and Ticatch, L. A., "Investigation of an Advanced Supersonic Fighter Concept Including Effects of Horizontal Tail and Canard Control Surfaces Over a Mach Number Range from 1.6 to 2.5," NASA TP 2526, May, 1986.

[20]Engquist, B. and Majda, A., "Absorbing Boundary Conditions for the Numerical Simulation of Waves," *Mathematics of Computation*, Vol. 31, July 1977, pp. 629–651.

Conference Proceedings from the 16th Congress of the **International Council of the Aeronautical Sciences (ICAS)**

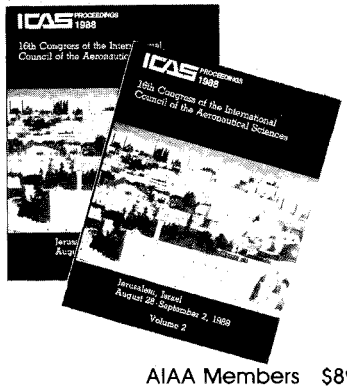

Held August 28 — September 2, 1988 in Jerusalem, Israel

2 volume set
1,900 pages August 1988
ISBN 0-930403-42-8

AIAA Members $89.50
Nonmembers $99.50
Order Number: 16-ICAS

The ICAS '88 conference proceedings bring you over 200 papers, representing work in 20 countries, on all branches of aeronautical science and technology. Published by the AIAA, this convenient 2-volume set gives you up-to-date information on:

- aerodynamics
- flight mechanics
- structures & propulsion
- aircraft design & operations
- systems technology
- hypersonics
- computer applications
- and more!

To Order: Write AIAA Order Department, 370 L'Enfant Promenade, S.W., Washington, DC 20024. Please include postage and handling fee of $4.50 with all orders. California and DC residents must add 6% sales tax on all orders. All orders under $50.00 must be prepaid. All foreign orders must be prepaid. Please allow 4-6 weeks for delivery.